IOPscience iopscience.iop.org

Home Search Collections Journals About Contact us My IOPscience

Growth and structure of $L1_0$ ordered FePt films on GaAs(001)

This article has been downloaded from IOPscience. Please scroll down to see the full text article.

2002 J. Phys.: Condens. Matter 14 12273

(http://iopscience.iop.org/0953-8984/14/47/304)

View the table of contents for this issue, or go to the journal homepage for more

Download details:
IP Address: 171.66.16.97
The article was downloaded on 18/05/2010 at 19:09

Please note that terms and conditions apply.

INSTITUTE OF PHYSICS PUBLISHING JOURNAL OF PHYSICS: CONDENSED MATTER

J. Phys.: Condens. Matter **14** (2002) 12273–12286 PII: S0953-8984(02)35969-1

Growth and structure of $L1_0$ ordered FePt films on GaAs(001)

A Nefedov[1], **T Schmitte**[1], **K Theis-Bröhl**[1], **H Zabel**[1], **M Doi**[2], **E Schuster**[2] **and W Keune**[2]

[1] Experimentalphysik/Festkörperphysik, Ruhr-Universität Bochum, Universitätstrasse 150, D-44780, Bochum, Germany
[2] Angewandte Physik, Gerhard-Mercator-Universität, Duisburg, D-47048 Duisburg, Germany

E-mail: Alexei.Nefedov@ruhr-uni-bochum.de

Received 18 April 2002, in final form 30 July 2002
Published 15 November 2002
Online at stacks.iop.org/JPhysCM/14/12273

Abstract

The structural properties of epitaxial $L1_0$ ordered FePt(001) films, grown by molecular beam epitaxy (alternating deposition of Fe and Pt atomic layers) on buffer-Pt/seed-Fe/GaAs(001) have been studied by *in situ* reflection high-energy electron diffraction and by *ex situ* x-ray scattering as a function of the growth conditions. Reflection high-energy electron diffraction intensity oscillations measured during FePt layer growth provide evidence for island growth at $T_s = 200\,^{\circ}$C and quasi layer-by-layer growth at $T_s = 350\,^{\circ}$C. From small-angle and wide-angle x-ray scattering it was found that the degree of epitaxy depends critically on morphology of the seed layer and the substrate roughness. X-ray diffraction analysis showed that the long-range order parameter increases from near zero for films grown at 200 °C to 0.65 for films grown at 350 °C. This confirms the fact that the order parameter is mainly determined by the surface mobility of the atoms which is controlled experimentally by the substrate temperature.

1. Introduction

Among thin film and superlattice systems exhibiting perpendicular magnetic anisotropy, the face centred tetragonal (fct) phases of binary alloys like CoPt, FePd and FePt, also referred to as CuAu(I) or $L1_0$ phases, have attracted much interest in recent years. This phase consists of a monatomically modulated superlattice of the two elements [1]. When grown with the monatomic layers parallel to the film plane, i.e. with the *c*-axis of the fct unit cell parallel to the film normal direction, this structure results in a perpendicular magnetic anisotropy. Fully ordered FePt is predicted to have one of the largest magnetic anisotropy energies (1.6×10^8 erg cm^{-3}) of any magnetic material [2, 3], and indeed, anisotropy energies of $K_u > 10^8$ erg cm^{-3} have been found experimentally in FePt films grown by molecular beam

 © 2002 IOP Publishing Ltd Printed in the UK

epitaxy (MBE) [4]. A large polar magneto-optical Kerr effect of 0.8° at 2 eV photon energy in FePt [5] makes these materials attractive candidates for media applications in magneto-optical recording. However, as was shown earlier [6], the magnetic properties of FePt are strongly correlated with the structural properties of the material, i.e. the crystallographic orientation of the film, the degree of chemical ordering and the degree of epitaxy.

Epitaxial growth of chemically ordered FePt thin films with the *c*-axis perpendicular to the film plane by MBE [4, 5, 7, 8] and by magnetron sputtering [6, 9, 10] has previously been demonstrated, and the observation of long-range chemical ordering at temperatures near 500 °C was attributed to enhanced surface diffusion during thin film growth. But all these films were grown on dielectric MgO substrates, while from the point of view of magnetoelectronics applications [11], the combination of metallic ferromagnets with semiconductors is preferable. Since the lattice parameter of GaAs is well matched to the in-plane lattice parameter of the FePt alloy with $L1_0$ structure (lattice mismatch is about 2.5%), it has been suggested that this substrate could be used for the growth of FePt films. However, alloying with the GaAs substrate limits the growth temperature to less than 350 °C. In our previous work [12] we demonstrated the room-temperature growth of epitaxial single Fe films on GaAs (001) without magnetic dead layers. Now we extend our experience to the fabrication of epitaxial multilayer structures, and we present a detailed investigation of the growth and the structural characterization of FePt films on GaAs(001). In a forthcoming paper the magnetic properties will be reported [13].

2. Sample preparation and *in situ* characterization

An ultrahigh vacuum (UHV) system (base pressure 9×10^{-11} mbar) for molecular beam epitaxy equipped with facilities for reflection high-energy electron diffraction (RHEED), low-energy electron diffraction (LEED) and Auger electron spectroscopy (AES) for *in situ* characterization was employed to prepare the samples. 'Epiready' GaAs(001) wafers 12 mm × 10 mm in size (with the longer side parallel to the $[1\bar{1}0]$ and the shorter side parallel to the [110] direction) were used as substrates. They were heated in UHV to 580 °C for 30 min, when oxygen desorption was observed by AES. Subsequently the substrate surface was further cleaned by Ar^+ sputtering (0.5 keV) at 600 °C for 30 min. After this, no surface impurities were detected by AES, and RHEED patterns (figure 1) and LEED images (figure 2) revealed the pseudo (4 × 6) surface reconstruction characteristic of the clean flat Ga-terminated GaAs(001) surface [11]. Subsequently, a thin Fe seed layer (of high-purity and natural isotope abundance) of 4.3 Å (samples 1 and 2) or 30 Å (sample 3) thickness was deposited onto the clean GaAs(001) surface at 50 °C to promote epitaxial growth. RHEED patterns were recorded during growth in periodic short time intervals by a CCD camera connected to the computer for data storage and subsequent analysis. This method allows the real-time monitoring of the film growth and of the in-plane atomic spacing [14]. The streaky RHEED patterns of the growing film indicate good epitaxial growth with flat surfaces, including the Pt(001) cap layer. Typical examples are shown in figure 3 taken during the growth of FePt film at 200 °C. The RHEED intensity (figure 3(b)) was drastically reduced after the deposition of the seed layer indicating surface disorder. However, the RHEED streak intensity (figure 3(c)) recovered after further deposition of a 60 Å thick (high-purity) Pt buffer layer, indicating epitaxial Pt growth with a flat surface. The Pt buffer follows the epitaxial relation Pt(001), [110] ∥ GaAs(001), [100]. The Pt buffer layer, the subsequently deposited FePt layer as well as a final 40 Å thick protective Pt cap layer were all grown at the same temperature. A few FePt films were prepared at different growth temperatures, but we restrict the present discussion to the three superlattices prepared at temperatures T_s, as presented in table 1. The FePt film structures were prepared by alternating evaporation of (nominally) monatomic layers of 2.0 Å thick Pt and 1.4 Å thick ^{57}Fe

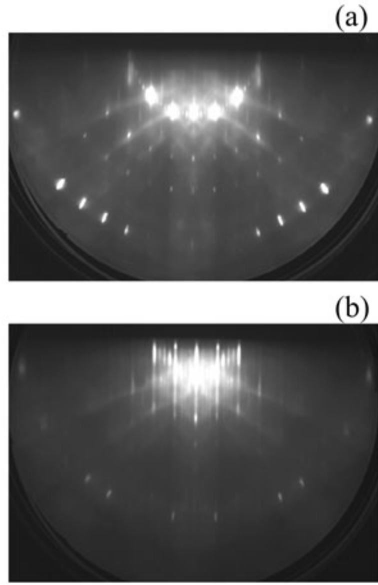

Figure 1. RHEED pattern of the clean GaAs(001)(4 × 6) substrate along the $[1\bar{1}0]$ azimuth (a) and the [110] azimuth (b) (electron energy: 10 keV).

Table 1. Growth temperature T_s (°C) as well as the values of the thicknesses t (Å) and roughnesses σ (Å) of corresponding layers obtained from the fit of the reflectivity data for three FePt films.

Sample	T_s	σ_{GaAs}	t_{seed}	σ_{seed}	t_{buf}	σ_{buf}	t_{FePt}	σ_{FePt}	t_{cap}	σ_{cap}
1	200	3.4	1.8	4.4	64.1	5.0	112.4	4.2	40.1	5.3
2	300	7.2	0.9	12.0	73.6	11.9	103.7	10.0	36.2	14.0
3	350	2.4	34.9	2.6	54.0	2.5	108.8	2.9	37.2	3.4

(isotopically enriched to 95%) from an electron gun and a home-built Knudsen cell with an Al_2O_3 crucible, respectively. (The use of ^{57}Fe allows Mössbauer effect measurements to be performed, as reported elsewhere [12].) Using this procedure the nominal $L1_0$ structure of the ordered FePt alloy is obtained. A total of 30 Fe/Pt bilayers was deposited, resulting in a total nominal thickness of the FePt alloy layer of ∼110 Å. The pressure during deposition was $<7.0 \times 10^{-10}$ mbar. The deposition rates (0.03 Å s^{-1} for Fe and ^{57}Fe, and 0.04 Å s^{-1} for Pt) were independently measured by calibrated quartz-crystal oscillators. Fe or Pt deposition was performed by computer-controlled alternating heating and cooling cycles of the corresponding evaporation sources. The deposition process included some periodic waiting times between the heating and cooling cycles. In case of sample 1 ($T_s = 200$ °C) the substrate was covered by a shutter during these waiting times, while no shutter was used during preparation of sample 2 ($T_s = 300$ °C) and sample 3 ($T_s = 350$ °C). We assume that this difference in shutter movement had no influence on multilayer growth and structure.

In order to obtain information on the FePt growth mode, the RHEED intensity in the diffuse scattering region around the specular beam was measured as a function of deposition time. Under such scattering conditions the intensity may be found to increase for half-monolayer coverage (rougher surface) and to decrease for complete monolayer (ML) coverage (smoother surface) [14]. The result is shown in figure 4(a) for growth at 200 °C (sample 1).

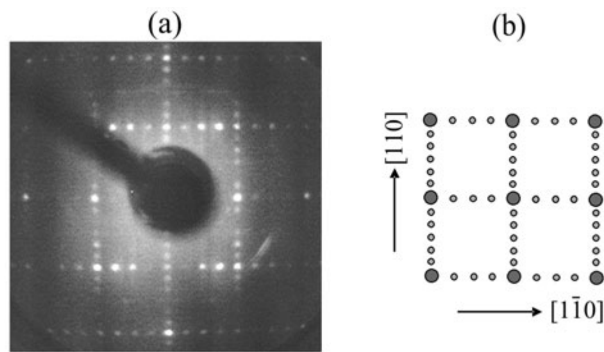

Figure 2. LEED pattern of the clean GaAs(001)(4 × 6) substrate (electron energy: 124 eV) (a) and schematics of the spot arrangement (b).

(The timescales of figures 4(a) and (b) give only the direct deposition time of the Fe and Pt layers respectively, i.e. the periodic waiting times of the closed shutter after each Fe or Pt deposition were subtracted from the total deposition time.) Periodic intensity oscillations are clearly observed. The period corresponds to 1 ML of Fe or Pt respectively, as determined via the quartz-crystal oscillator. Obviously the intensity increases during Fe deposition, while it is reduced during Pt deposition. This demonstrates that upon arrival of Fe atoms the surface becomes atomically rougher due to Fe island formation, while the subsequently deposited Pt atoms smooth the surface, presumably by filling the voids between Fe islands. Apparently the growth temperature of 200 °C is not yet sufficiently high to promote Fe surface diffusion which would lead to an atomically smooth surface. We conclude that a rather imperfect $L1_0$ structure is formed at $T_s = 200\,^\circ$C, in agreement with our x-ray scattering results (see section 3.2). In contrast, FePt film growth at 350 °C results in quasi layer-by-layer growth of Fe and Pt. This is inferred from figure 4(c), where periodic RHEED intensity oscillations are observed. In this case the RHEED intensity was measured close to the specular spot position, where the intensity decreases for half-monolayer coverage (rough surface) and increases for complete ML coverage (smooth surface) [14]. (The timescales in figure 4(c) and 4(d) give the total deposition time of the multilayer, including the periodic waiting time during cooling/heating cycles of the evaporators.) The deep minima observed in figure 4(c) correspond to half-monolayer coverage of Fe and Pt respectively, implying maximum roughness. Above and below half-monolayer coverage the intensity increases for Fe as well as Pt, corresponding to surface smoothing. We conclude that a more perfect $L1_0$ ordered structure is grown at $T_s = 350\,^\circ$C, in agreement with our x-ray data (section 3).

Since the in-plane lattice parameter (spacing) is inversely proportional to the distance between the RHEED reflections in reciprocal space, the evolution of the spacing relative to that of the Pt buffer layer has been determined from the deposition-time dependence of the separation of the RHEED reflections. The peak position of the RHEED spot intensity was obtained from an intensity scan across the reflections in the horizontal direction in figure 3. The peak positions were accurately determined by a least-squares fit of the experimental intensity scan with Gaussians and a parabolic background [14]. The result is shown in figures 4(b) and (d) for $T_s = 200$ and 350 °C respectively. For $T_s = 200\,^\circ$C, large oscillations of the in-plane lattice spacing versus the Fe/Pt deposition time are evident; the oscillations are centred near the relative lattice spacing of the $L1_0$ ordered FePt alloy. These oscillations provide evidence for island growth at 200 °C, i.e. incomplete layer-by-layer growth or incomplete $L1_0$

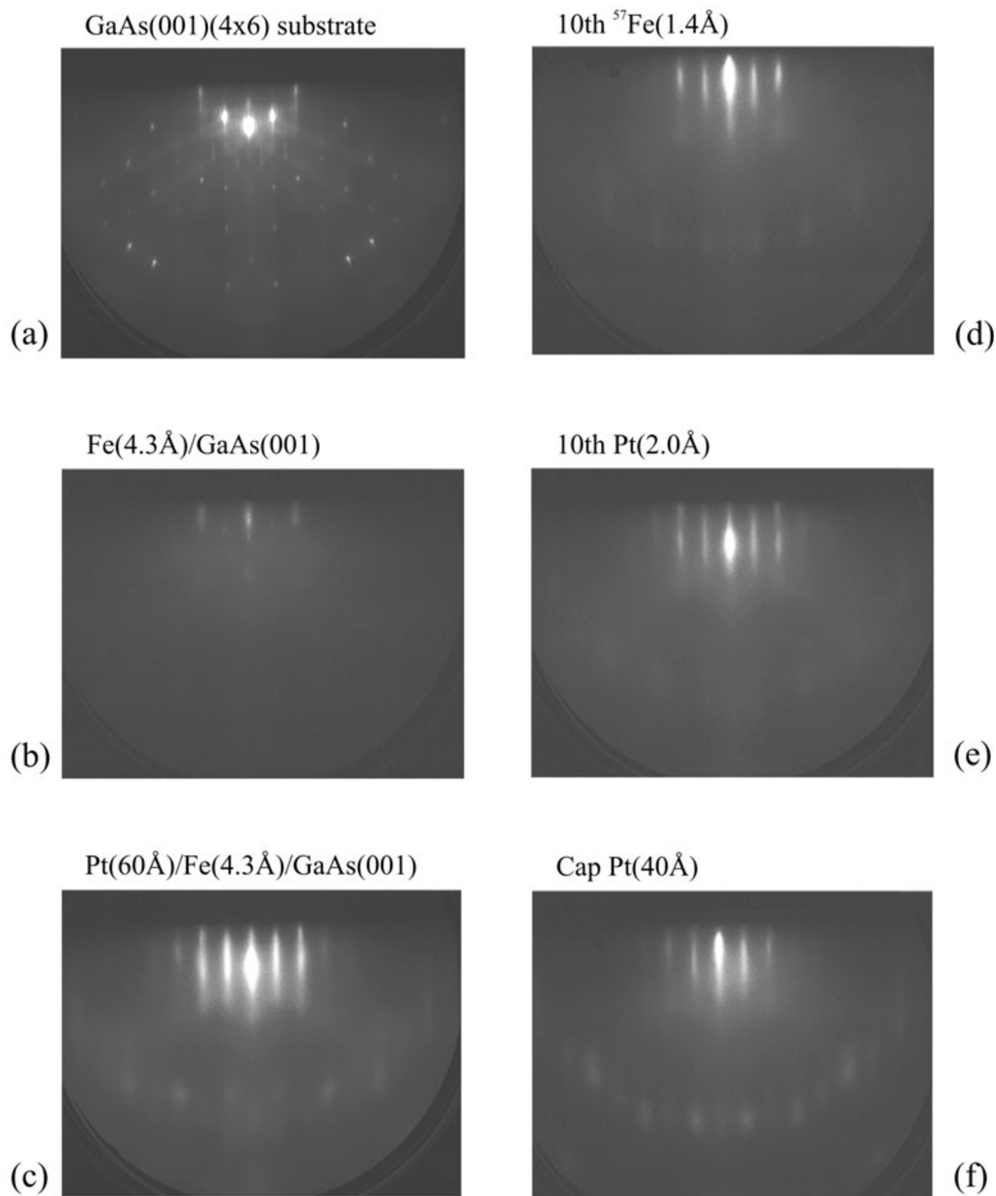

Figure 3. RHEED patterns along the $[1\overline{1}0]$ azimuthal direction of (a) a clean GaAs(001)(4 × 6) substrate and after sequential deposition of: (b) a 4.3 Å thick Fe seed layer grown at 50 °C; (c) a 60 Å thick Pt buffer layer, (d) the 10th atomic layer of ^{57}Fe, (e) the 10th atomic layer of Pt, (f) a 40 Å thick Pt cap layer. Growth temperature for (c)–(f): $T_s = 200\,°C$ (electron energy: 10 keV).

structure, in agreement with our conclusions drawn from the RHEED intensity oscillations. It is well established that in-plane lattice parameter oscillations during film growth may occur in heteroepitaxial systems with a lattice misfit between film and substrate [15, 16]. For instance, for Co/Cu the growing Co monolayers are periodically in-plane relaxed (contracted) for half-integer coverages (i.e. for maximum roughness) [15]. In the case of 45°-rotated growth of

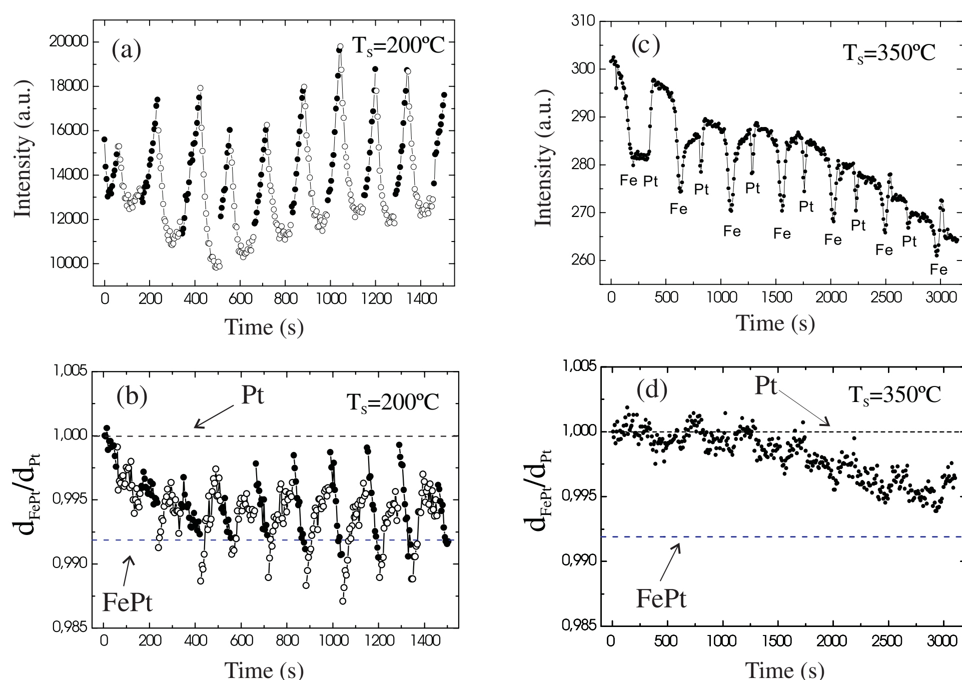

Figure 4. Deposition-time dependence during FePt film growth of: (a) diffusely scattered RHEED intensity, (c) specular RHEED intensity, (b) and (d) relative in-plane interplanar distance d_{FePt}/d_{Pt}. (a), (b) $T_s = 200\,^{\circ}$C (sample 1), (c), (d) $T_s = 350\,^{\circ}$C (sample 3). In (a) and (b): ●—deposition of Fe monolayer, ○—deposition of Pt monolayer. Dashed lines in (b) and (d) correspond to bulk values of Pt and FePt interplanar distance.

Fe(001) and Pt(001), the in-plane lattice misfit amounts to 3%, if the bulk lattice spacings are used. However, even for homoepitaxial growth, e.g. Cu on Cu(001), in-plane lattice parameter oscillations have been reported [15]. In this case in-plane lattice relaxation at the surface of a Cu island may occur due to the different chemical bonding situation (intrinsic surface stress tensor and renormalized surface energy [17]) at the very surface. Further investigations are necessary for fully understanding details of the oscillations in figure 4(b). For 350 °C growth, by contrast, the in-plane lattice parameter of the growing superlattice does not show significant oscillations (figure 4(d)). With increasing deposition time the lattice parameter first remains constant at the corresponding value of the Pt buffer layer up to three bilayers and then the following decrease take place. This reflects the more perfect growth of the $L1_0$ structure at 350 °C.

3. *Ex situ* structural characterization

The basic structural analysis was performed using a Philips PW 1730 diffractometer with a graphite monochromator or a medium-resolution diffractometer attached to a 12 kW rotating anode generator (Cu Kα radiation, λ = 1.542 Å), while x-ray diffraction data for the determination of the order parameter were obtained using synchrotron radiation at the W1.1 beamline of HASYLAB with the wavelength $\lambda = 1.512$ Å.

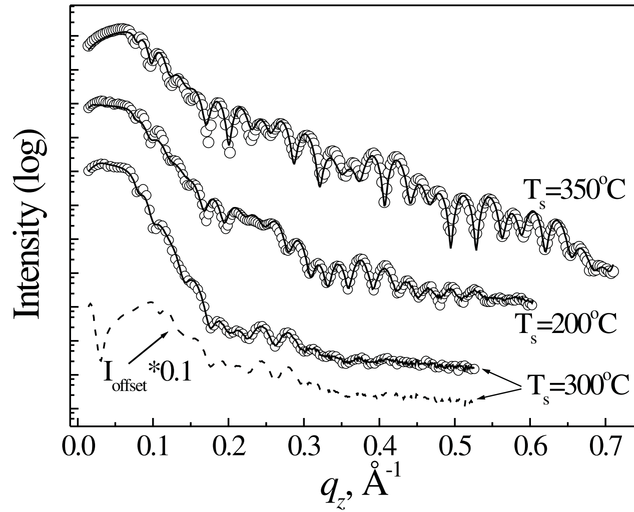

Figure 5. The reflectivity data for all samples with a logarithmic intensity scale versus the scattering vector $\boldsymbol{q_z} = 4\pi \sin\theta/\lambda$. The full curves show fits with parameters presented in table 1. Curves are shifted vertically with respect to each other by a factor 10^2. The offset scan ($\Delta\theta = 0.2°$) for the sample 2 ($T_s = 300$ °C) is shifted downwards by a factor of 10 for better visibility (dashed curve).

3.1. X-ray reflectivity studies

X-ray scattering is most suitable for a detailed structural characterization of thin films and multilayers, since it is a non-destructive method providing surface as well as subsurface information on one and the same sample. Information about the film thickness, the interfacial roughnesses and the electron density profile perpendicular to the film plane irrespective of the crystallinity of the film is obtained via specular and off-specular scans in the small-angle regime (reflectivity measurements). Assuming a certain electron density profile, the reflectivity can be calculated as a function of the scattering vector. In this work we calculated the x-ray reflectivity by means of a dynamical treatment, generally referred to as the Parratt formalism for x-ray reflectivity [18], using optical boundary conditions for reflection, refraction and transmission at each interface. The Parratt formulae were modified according to Névot and Croce [19] to take the roughness into account, which is modelled by the root mean square of the electron density height fluctuation at the interfaces. For fitting of our data we used a model sample consisting of a substrate (GaAs), iron seed and platinum buffer layers, one FePt layer with a density $\rho = 15.15$ g cm^{-3} [20] and a Pt cap layer. We also tested a model taking into account a multilayer structure for the FePt layer, but an improvement of the fit was not achieved, while the time of the fitting procedure drastically increased.

The reflectivity data for all samples are shown in figure 5 with a logarithmic intensity scale. The open circles represent the data points and the full lines are fits with parameters presented in table 1. In figure 6 we show a series of off-specular transverse scans at different q_z values for samples 2 and 3. It can clearly be seen that the transverse scans consist of two components: a specular and a diffuse component. Moreover, for sample 2 we find that the specular part vanishes completely at $q_z \approx 0.18$ Å^{-1} and at higher q_z values the reflectivity curve for this sample consists only of diffuse intensity. This is also seen by comparing the reflectivity curve with the offset ($\theta + \Delta\theta - 2\theta$) scan with $\Delta\theta = 0.2°$ for sample 2 ($T_s = 300$ °C) (dashed curve in figure 5). Therefore, the diffuse non-specular intensity has to be subtracted

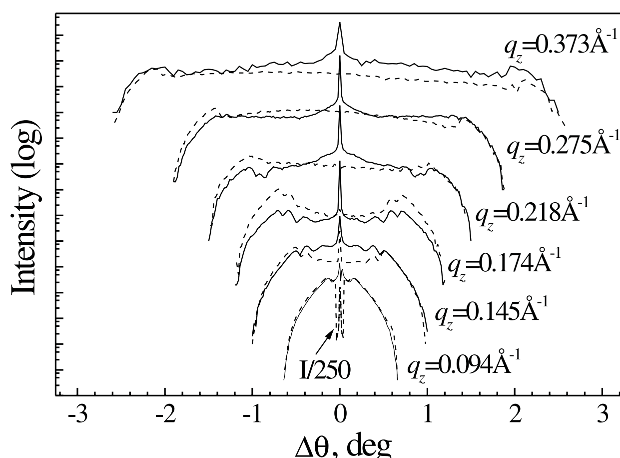

Figure 6. Transverse scans (rocking curves) for samples 2 (dashed curves) and 3 (full curves) at different q_z values. Curves are shifted vertically by a factor 10^2.

from the data before starting the fitting procedure of the specular reflectivity. Within errors bars of the fitting parameters, which are no more than 5% in our case, and taking into account the listed values for the interface roughness, the layer thicknesses (see table 1) practically coincide with the nominal values estimated from the growth conditions. Discrepancies are only seen for the seed layer thicknesses of samples 1 and 2. Those cannot be reliably defined, because their thickness is of the same order as their roughness. From the fits a clear tendency can be recognized: within a sample the roughness values of all interfaces stay practically constant from bottom to top, indicating that the roughness of the interfaces is mainly determined by the roughness of the substrate and the seed layer morphology. Furthermore, the shape of the diffuse component of the rocking curves (see figure 6) is typical for multilayers with correlated roughnesses. Therefore we conclude that the growth of all layers takes place by replicating the surface profile of the previous layer.

3.2. Out-of-plane diffraction

The wide-angle radial scans across a reciprocal lattice point (Bragg scans) normal to the growth direction provide information about the structural coherence of the films (polycrystalline versus single crystalline) and in the latter case also about the predominant texture. The Bragg scans for three FePt films are presented in figure 7(a) demonstrating the evolution of the superstructure (001) and (003) Bragg peaks of the $L1_0$ ordered FePt structure with increasing growth temperature T_s as compared with the fundamental (002) and (004) reflections of FePt alloy. In spite of the strong overlap of the FePt(002) fundamental peak and the Pt(002) buffer layer reflections in figure 7(a), together with the relatively poor resolution of a conventional diffractometer, it is nevertheless possible to establish the tendency of increasing $L1_0$ order with increasing growth temperature. In order to determine in detail the structure of the FePt films and to calculate precisely values of S, out-of-plane Bragg scans have been carried out using synchrotron radiation which provides a higher intensity and better resolution than laboratory x-ray sources. The Bragg peaks, corresponding to the (001) superstructure reflection and the (002) fundamental reflection of ordered FePt alloys with $L1_0$-type crystal structure, are shown in figures 7(b) and (c) respectively. From the width of the FePt(001) Bragg peak we determined the chemical coherence length along the surface normal to be $\approx$70 Å for sample 2 and $\approx$75 Å for

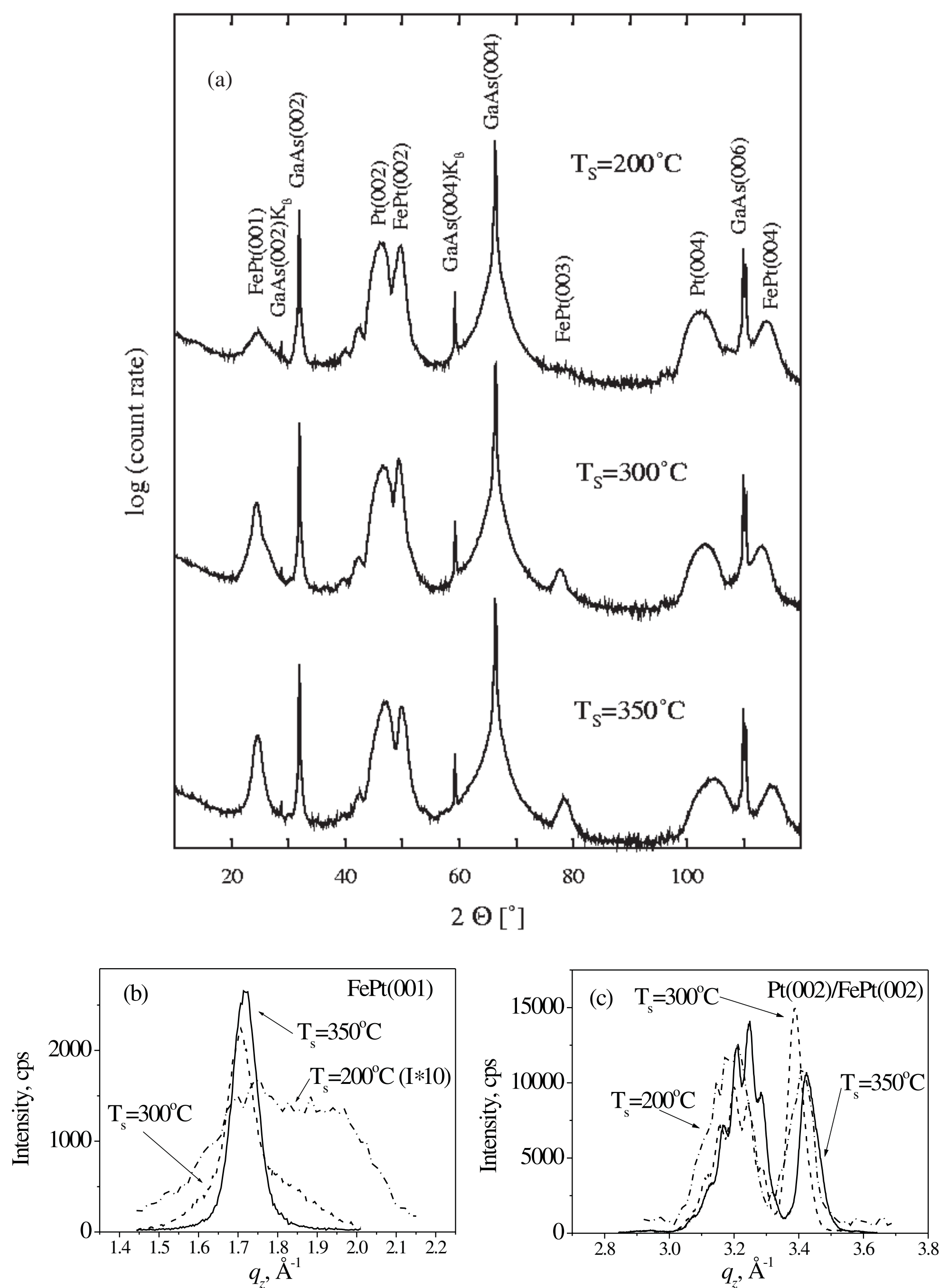

Figure 7. X-ray diffraction patterns ($\theta - 2\theta$ scans) of FePt films grown at (a) $T_s = 200\,^\circ$C (sample 1), $T_s = 300\,^\circ$C (sample 2) and $T_s = 350\,^\circ$C (sample 3) (Cu Kα radiation). Radial scans of superstructure FePt(001) (b) and fundamental FePt(002) Bragg peaks (c) carried out with the use of synchrotron radiation for samples 1 (chain curve), 2 (dashed curve) and 3 (full curve).

sample 3. For sample 2 a second broad FePt(001) component can be recognized as well (figure 7(b)), indicating the presence of chemically ordered FePt grains with a size of about 25 Å. For sample 1 the sharp component of the FePt(001) peak is missing. Instead, a broad component with a smaller intensity is observed, demonstrating a poor chemical long-range order. The rocking width of the FePt(001) peaks is about $3.9 \pm 0.1°$ for all three samples. In figure 7(c) the fundamental (002) reflection from FePt was placed at $q_z = 3.388$ Å^{-1} for sample 2 ($T_s = 300$ °C) and at $q_z = 3.424$ Å^{-1} for sample 3 ($T_s = 350$ °C). The corresponding lattice parameters in the direction normal to the surface are $c = 3.710 \pm 0.005$ and 3.670 ± 0.005 Å for samples 2 and 3 respectively. The first value is close to the bulk lattice parameter of ordered FePt alloys ($c = 3.724$ Å) [20]. This indicates a slight compression of the lattice in the film growth direction only. For sample 3 the compression is much bigger. The difference in the out-of-plane lattice parameters for samples 2 and 3 can be understood, if we take into account the interface roughness obtained from the reflectivity measurements (table 1). The rougher interface allows more lattice relaxation than the smooth interface. This notion is confirmed by the film grown at $T_s = 350$ °C with a 30 Å Fe seed layer, for which we find a sharp interface ($\sigma = 2.5 \pm 0.1$ Å) and a concomitant out-of-plane compression. In this case we expect an in-plane expansion of both, the Pt buffer layer and the FePt superlattice, which indeed has been confirmed by in-plane diffraction experiments, to be discussed further below. The problem of the mismatch between the Pt and the FePt in-plane lattice parameters for sample 2 is solved by the presence of small grains of the $L1_0$ phase. From the width of the FePt(002) Bragg peaks we can calculate the structural coherence length along the surface normal, which is 97 and 84 Å for films grown at $T_s = 300$ and 350 °C, respectively. This implies that the structural coherence is slightly larger than the chemical coherence of the $L1_0$ structure. The mosaic spreads of the FePt(002) Bragg peaks are 1.68°, 1.65°, and 1.45° for samples 1, 2 and 3 respectively.

The peaks to the left of the FePt(002) peaks (figure 7(c)) correspond to the diffraction from the Pt buffer and cap layers. The shape of these Pt(002) peaks can be explained by interference effects between beams diffracted from the buffer and the cap platinum layers. Since these effects are not the subject of our present study, we will not analyse them in detail. We mention here only that within the experimental error bars the Pt(002) peak position (the main maximum) for samples 1 and 2 corresponds to the bulk value of the Pt(002) lattice parameter. The peak position for sample 3 is shifted to high q_z values, indicative of compression of the lattice in the growth direction as already noticed for the FePt(002) Bragg peak of this sample. A small peak at $q_z = 3.26$ Å^{-1} for the sample grown at $T_s = 350$ °C indicates the presence of a small number of FePt(200) grains with the tetragonal c-axis being in the plane of the film. Their presence most likely serves the purpose of reducing the mismatch between the Pt seed layer and the FePt film. The misorientation of some of the grains may also explain the smaller intensity of the FePt(002) Bragg peak for sample 3 as compared with sample 2.

3.3. Order parameter

Integration of the FePt(00L) peak areas yields a one-dimensional chemical order parameter S, which can be defined as [21]

$$S = \frac{r_{\mathrm{Fe}} - x_{\mathrm{Fe}}}{y_{\mathrm{Pt}}} = \frac{r_{\mathrm{Pt}} - x_{\mathrm{Pt}}}{y_{\mathrm{Fe}}}. \qquad (1)$$

Here $x_{\mathrm{Fe(Pt)}}$ is the atomic fraction of Fe(Pt) in the sample, $y_{\mathrm{Fe(Pt)}}$ is the fraction of Fe(Pt) sites, and $r_{\mathrm{Fe(Pt)}}$ is the fraction of Fe(Pt) sites occupied by the correct atomic species. S reaches unity for perfectly ordered films of the stoichiometric composition, $Fe_{50}Pt_{50}$, and is zero for a chemically disordered film. The area of either a fundamental or a superstructure peak can be

Table 2. Parameters used to estimate the chemical order parameter S of FePt (LP is the Lorentz polarization factor, e^{-M} is the Debye–Waller correction and f and δ are the real and imaginary parts of the atomic scattering factors).

Peak	Q (Å^{-1})	LP	M_{Fe}	f_{Fe}	δ_{Fe}	M_{Pt}	f_{Pt}	δ_{Pt}
(001)	1.70	2.05	0.005	22.2	3.4	0.005	71.2	8
(002)	3.40	0.6	0.019	17.5	3.3	0.018	59.4	7

expressed as

$$A \propto (LP)FF^*, \tag{2}$$

where LP is the Lorentz polarization factor for a single crystal [22], and F and F^* are the structure factor and its complex conjugate, respectively. For the $L1_0$ structure we have

$$(FF^*)_{fund} = 16[(x_{Fe} f_{Fe} e^{-M_{Fe}} + x_{Pt} f_{Pt} e^{-M_{Pt}})^2 + (x_{Fe}\delta_{Fe} e^{-M_{Fe}} + x_{Pt}\delta_{Pt} e^{-M_{Pt}})^2] \tag{3}$$

$$(FF^*)_{super} = 4S^2[(f_{Fe} e^{-M_{Fe}} + f_{Pt} e^{-M_{Pt}})^2 + (\delta_{Fe} e^{-M_{Fe}} + \delta_{Pt} e^{-M_{Pt}})^2] \tag{4}$$

for the fundamental and the superstructure peaks respectively. e^{-M} is the Debye–Waller correction and f and δ are the real and imaginary parts of the atomic scattering factors. Therefore, the chemical order parameter can be extracted directly from the ratio of the integrated areas of the fundamental (002) and of the superstructure (001) peaks. Because of differences in the mosaic spread of the fundamental and superstructure peaks, the mosaic spread of each of the peaks was included in the calculation. We assumed that $x_{Fe} = x_{Pt} = 0.5$, and using the values for Fe and Pt of these parameters for the different diffraction peaks as listed in table 2, we find $S = 0.60 \pm 0.05$ and $S = 0.65 \pm 0.05$ for samples 2 and 3 respectively. Sample 1 exhibits a very small (001) peak intensity, therefore the uncertainty of the order parameter is large. But we estimate S to be smaller than 0.1.

3.4. In-plane diffraction

The out-of-plane Bragg scans discussed so far only probe the texture normal to the film plane and nothing can be concluded from these scans about the in-plane structure. Since information on the degree of epitaxy is very important, Bragg scans have been carried out in surface scattering geometry as well, i.e. with glancing incident and exit angles to the surface, in order to determine the epitaxial relationship between film and substrate, the strain and lattice mismatch, and the average domain size in directions parallel to the surface. In our experiments the angle of incidence α_i was kept constant at about the critical angle for total external reflection from platinum. The vertical slit of the detector was open, resulting in an integration over the exit angle α_f. Figure 8 shows the result of an ω-scan of sample 3, where the sample is rotated about an axis parallel to the film normal, while the detector is kept fixed at the FePt(200) Bragg position ($Q = 3.22$ Å^{-1}). Four peaks separated by 90° are detected corresponding to the (200), (020), ($\bar{2}$00) and (0$\bar{2}$0) FePt reflections, revealing the four-fold symmetry. Scans like the one shown in figure 8 were also carried out for the FePt(220) Bragg position. These scans allow us to determine the epitaxial relationships between the FePt film and the substrate. It was found that the FePt(Pt)$\langle 110\rangle$ axis is aligned parallel to the $\langle 100\rangle$ axis of GaAs and the FePt(Pt)$\langle 100\rangle$ axis is parallel to the $\langle 1\bar{1}0\rangle$ axis of GaAs, i.e. there is a 45° epitaxy between FePt and GaAs as we had already concluded from the RHEED pattern in figure 3.

Figure 9 shows the radial scans through the FePt(200) Bragg peaks for samples 2 (dashed curve) and 3 (full curve). The Bragg peak on the left-hand side at $Q = 3.130$ Å^{-1} corresponds to the diffraction from the GaAs substrate and the peak at $Q = 3.157$ Å^{-1}

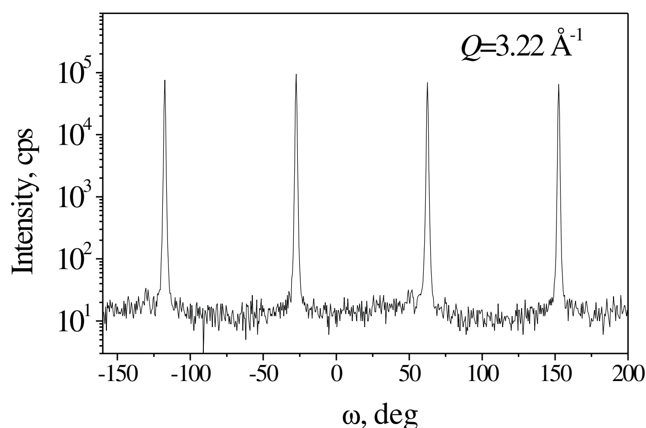

Figure 8. The rotational or ω scan of the FePt(200) in-plane reflection for sample 3. The reflections are separated by 90°, indicating the four-fold symmetry.

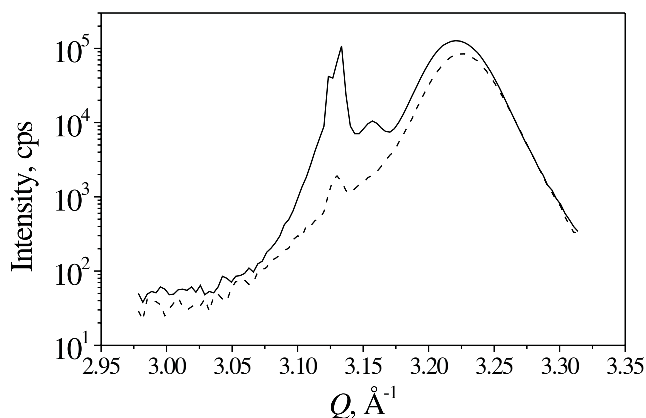

Figure 9. The radial scans through the FePt(200) Bragg peak for samples 2 (dashed curve) and 3 (full curve).

for sample 3 corresponds to the expanded Pt buffer layer with the in-plane lattice parameter $d_{100} = 3.98 \pm 0.01$ Å. The presence of this peak for the sample grown at $T_s = 350\,°\mathrm{C}$ confirms our conclusion about the in-plane expansion of the Pt buffer layer. A small increase in the background takes place near $Q = 3.20$ Å^{-1} for both samples, which could be caused by the diffraction from the Pt layer with the bulk lattice parameter. Scans like that shown in figure 9 were also carried out for the FePt(020) Bragg position, which allow us to determine the interplanar distance (the lattice parameter) for the FePt layer in two orthogonal directions parallel to the surface. We find that both in-plane lattice parameters are equal to each other: $a = b = 3.910 \pm 0.005$ Å for the FePt superlattice grown at 350 °C and $a = b = 3.885 \pm 0.005$ Å for the one grown at 300 °C. The in- and out-of-plane lattice parameters determined by x-rays are in complete agreement with the expected Poisson behaviour. Finally, from the width of these radial scans we estimated the in-plane coherence length to be about 70 Å for both samples.

4. Conclusions

In conclusion, ordered (001)-oriented FePt films with $L1_0$ (CuAu (I)) structure have been grown on Pt-buffer/Fe-seed/GaAs(001) substrates by MBE with alternating deposition of Fe and Pt atomic layers at different substrate temperatures. RHEED intensity oscillations measured during FePt film growth provide evidence for Fe and Pt island growth at $T_s = 200\,°\mathrm{C}$ and quasi layer-by-layer growth at $T_s = 350\,°\mathrm{C}$. From *ex situ* x-ray reflectivity measurements we found that the roughness value of all interfaces is determined mainly by the roughness of the substrate, and from the shape of the rocking curves it is established that the growth of all layers takes place via replicating the surface profile from the previous layer. The lattice parameters obtained from the out-of-plane and in-plane Bragg scans indicate an in-plane expansion of the FePt lattice with a corresponding compression in the growth direction, which are in agreement with the expected Poisson behaviour. The difference in the lattice parameters for the samples grown at $T_s = 300$ and $350\,°\mathrm{C}$ is explained by the difference of the interface roughnesses, because the rougher interface allows larger lattice relaxation than the smooth interface. Therefore we conclude that the degree of epitaxy depends critically on the seed layer morphology and the substrate roughness. From RHEED pattern and in-plane ω-scans we determined that a 45° epitaxy takes place between FePt and GaAs. We calculated the long-range order parameter of FePt layers, which is nearly zero for growth at 200 °C, and increases to 0.65 ± 0.05 at 350 °C. This confirms the conclusions made in [7] that the order parameter is mainly determined by the surface mobility, which is controlled experimentally by the substrate temperature during growth.

Acknowledgments

Technical assistance by U von Hoersten (Duisburg) is highly appreciated. Financial support by the Deutsche Forschungsgemeinschaft under SFB491 is gratefully acknowledged.

References

[1] Massalski T B 1990 *Binary Alloy Phase Diagrams* 2nd edn (Metals Park, OH: ASM International)
[2] Daalderop G H, Kelley P J and Schuurmans M F H 1991 *Phys. Rev.* B **44** 1254
[3] Sacuma A 1994 *J. Phys. Soc. Japan* **63** 3053
[4] Farrow R F C, Weller D, Marks R F and Toney M F 1996 *J. Appl. Phys.* **79** 5967
[5] Cebollada A, Weller D, Sticht J, Harp G R, Farrow R F C, Marks R F, Savoy R and Scott J C 1994 *Phys. Rev.* B **50** 3419
[6] Thiele J U, Folks L, Toney M F and Weller D 1998 *J. Appl. Phys.* **84** 5686
[7] Farrow R F C, Weller D, Marks R F, Toney M F, Horn S, Harp G R and Cebollada A 1996 *Appl. Phys. Lett.* **69** 1166
[8] Shima T, Moriguchi T, Mitani S and Takanashi K 2002 *Appl. Phys. Lett.* **80** 288
[9] Lairson B M, Visokay M R, Sinclair R and Clemens B M 1993 *Appl. Phys. Lett.* **62** 639
[10] Watanabe M and Homma M 1996 *Japan. J. Appl. Phys.* Part 2 **35** L1264
[11] Zölfl M, Brockmann M, Köhler M, Kreuzer S, Schweinböck T, Miethaner S, Bensch F and Bayreuther G 1997 *J. Magn. Magn. Mater.* **175** 16
[12] Doi M, Roldan Cuenya B, Keune W, Schmitte T, Nefedov A, Zabel H, Spoddig D, Meckenstock R and Pelzl J 2002 *J. Magn. Magn. Mater.* **240** 407
[13] Doi M, Schuster E, Keune W, Schmitte T, Gök S, Theis-Bröhl K, Nefedov A and Zabel H, in preparation
[14] Schatz A and Keune W 1999 *Surf. Sci.* **440** L841
[15] Fassbender J, May U, Schirmer B, Jungblut R M, Hillebrands B and Güntherodt G 1995 *Phys. Rev. Lett.* **75** 4476
[16] Massies J and Grandjean N 1993 *Phys. Rev. Lett.* **71** 1411
[17] Shchukin V A and Bimberg D 1999 *Rev. Mod. Phys.* **71** 1125

[18] Parratt L G 1954 *Phys. Rev.* **95** 359
[19] Névot L and Croce P 1980 *Rev. Phys. Appl.* **15** 761
[20] 1971 *Numerical Data and Functional Relationships in Science and Technology Landolt-Börnstein New Series* Group III vol 6 (Berlin: Springer) p 571
[21] Warren B E 1990 *X-Ray Diffraction* (New York: Dover) p 208
[22] Warren B E 1990 *X-Ray Diffraction* (New York: Dover) p 44